This is the accepted manuscript made available via CHORUS. The article has been published as:

Quark-flavored scalar dark matter

Bhubanjyoti Bhattacharya, David London, James M. Cline, Alakabha Datta, and Grace Dupuis

Phys. Rev. D **92**, 115012 — Published 15 December 2015

DOI: 10.1103/PhysRevD.92.115012

UdeM-GPP-TH-15-244, UMISS-HEP-2015-03

Quark-flavored scalar dark matter

Bhubanjyoti Bhattacharya* and David London†
Physique des Particules, Université de Montréal, C.P. 6128, succ. centre-ville, Montréal, QC, Canada H3C 3J7

James M. Cline‡
Department of Physics, McGill University, 3600 Rue University, Montréal, Québec, Canada H3A 2T8 and Niels Bohr International Academy, University of Copenhagen, Blegdamsvej 17, DK-2100, Copenhagen, Denmark

Alakabha Datta§
Department of Physics and Astronomy, University of Mississippi, Lewis Hall, University, Mississippi, 38677 USA

Grace Dupuis¶
Department of Physics, McGill University, 3600 Rue University, Montréal, Québec, Canada H3A 2T8

It is an intriguing possibility that dark matter (DM) could have flavor quantum numbers like the quarks. We propose and investigate a class of UV-complete models of this kind, in which the dark matter is in a scalar triplet of an SU(3) flavor symmetry, and interacts with quarks via a colored flavor-singlet fermionic mediator. Such mediators could be discovered at the LHC if their masses are ~ 1 TeV. We constrain the DM-mediator couplings using relic abundance, direct detection, and flavor-changing neutral-current considerations. We find that, for reasonable values of its couplings, scalar flavored DM can contribute significantly to the real and imaginary parts of the B_s-$\bar{B}_s$ mixing amplitude. We further assess the potential for such models to explain the galactic center GeV gamma-ray excess.

1. INTRODUCTION

In recent years, model builders have entertained the idea that dark matter (DM) comes in three generations like the matter particles of the standard model (SM), and that its interactions with the SM are governed by an approximate flavor symmetry. In the design of such a model, one must decide whether the dark matter carries quark or lepton flavor. In this paper we focus on quark-flavored dark matter, which has previously been studied in refs. [1]-[10]. A common element of such models is the presence of an additional new particle, the mediator that carries the quantum numbers of the standard model quarks, to which the dark matter couples.

One must also decide whether the dark matter is a fermion or a scalar (implying the opposite choice for the mediator). So far, previous studies have assumed the former, which we refer to as FDM. The scalar case, which we call SFDM, has some distinctive features that deserve investigation; we aim to fill this gap in the present paper. One difference is that the colored fermionic mediators χ have a larger production cross section at the Large Hadron Collider, improving the prospects for their discovery or tightening constraints on their masses relative to scalar mediators.

Another difference is that scalar DM ϕ can couple to the Higgs by the renormalizable operator $\lambda|\phi|^2|H|^2$ that leads to Higgs portal interactions. We will show that this naturally dominates over the mediator interactions for setting the relic abundance and indirect signals for light dark matter, putting SFDM on a similar footing to minimal scalar dark matter in these respects. However, for heavy DM with mass $m_\phi \sim$ 450-1000 GeV, mediator exchange with annihilation to $t\bar{t}$ can dominate over Higgs portal annihilations. Moreover, the mediator exchanges can lead to important effects for direct detection and flavor-changing neutral-current (FCNC) processes.

A further motivation for our study arises from indications of an excess of multi-GeV energy gamma rays from the galactic center (GC), whose origin is not obviously tied to known astrophysical sources [11–16]. There has been considerable interest in dark matter annihilations into standard model particles as a possible explanation of the signal, including FDM models [8]. Here we update the status of scalar dark matter annihilations through the Higgs portal to fit the GC excess, taking account of newer data sets provided by refs. [16, 17].

In the following we define the models (section 2), derive constraints on the mediator masses/couplings (m_χ and Λ_{ij}) from the LHC (section 3), and show the implications for the couplings from requiring a thermal origin for the abundance (section 4). Constraints from indirect detection, as well as the tentative evidence for the GC excess, are examined in section 5, followed by a study of direct detection (section 6). Additional bounds on m_χ and Λ_{ij} from FCNC searches are presented in section 7.

*bhujyo@lps.umontreal.ca
†london@lps.umontreal.ca
‡jcline@physics.mcgill.ca
§datta@phy.olemiss.edu
¶dupuisg@physics.mcgill.ca

In section 8 we illustrate the range of possible effects in this model A summary of our findings is given in the concluding section 9.

2. MODELS

The largest quark flavor symmetry group is a product of three SU(3)'s, $\mathrm{SU}(3)_Q \times \mathrm{SU}(3)_u \times \mathrm{SU}(3)_d$, where Q denotes quark doublets and u, d the weak singlets. If we took the dark matter triplet to transform under one of these SU(3)'s, it would be natural to invoke minimal flavor violation (MFV) [18] to suppress FCNCs in our model. However, this transformation choice is not necessary; it is more general to assume that the DM transforms under its own $\mathrm{SU}(3)_\phi$ group [19], which like the others gets spontaneously broken by the mechanism that generates the Yukawa couplings. We adopt this more general approach here.

This leads to three possible models, characterized by the quantum numbers of the mediator particle χ. All of them have interactions of the form

$$\Lambda_{ij}\, \phi_i^*\, \bar{\chi} P_{L,R} q_j + \text{h.c.}\ , \tag{1}$$

where q_j stands for quark doublet Q_j or singlets u_j, d_j, and $P_{L,R}$ projects onto left- or right-handed states (left for Q_j and right for u_j, d_j). We will denote the models by Q, u, d, according to the kind of quarks which appear in (1), and which the mediator must resemble in most respects. The differences are that the mediator has no generation index, and it is vector-like, having a mass $m_\chi \gtrsim 1$ TeV (see sect. 3 below) that is independent from electroweak symmetry breaking.

In addition to the interactions with quarks, scalar dark matter can couple to the Higgs via

$$\lambda_{ij}\, \phi_i^* \phi_j\, |H|^2\ , \tag{2}$$

where λ_{ij} is Hermitian. At scales above that where flavor symmetry is broken, one expects the flavor-symmetric form $\lambda_{ij} = \lambda_0\, \delta_{ij}$, but this gets flavor-breaking radiative corrections that we will discuss below.

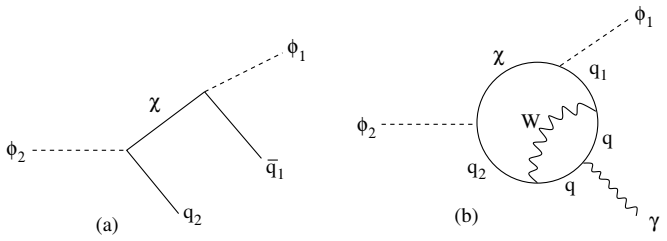

Figure 1: Decay of the heavy DM state to the lightest one: (a) tree-level diagram for $\phi_2 \to q_2 \bar{q}_1 \phi_1$; (b) two-loop diagram for $\phi_2 \to \phi_1 \gamma$.

2.1. DM mass spectrum and couplings

Like the coupling (2), we expect the mass matrix for scalar triplet dark matter to be flavor-conserving at high scales, but corrected by flavor-breaking self-energies at one loop, and also by the contribution from (2) due to electroweak symmetry breaking:

$$(m_\phi^2)_{ij} = m_0^2\, \delta_{ij} + m_1^2\, (\Lambda\Lambda^\dagger)_{ij} + v^2 \lambda_{ij} + \dots\ , \tag{3}$$

where $v = 174$ GeV is the VEV of the complex Higgs field. *A priori,* there are no restrictions on the structure of Λ_{ij} nor do we know whether m_0^2 dominates over the other contributions. For simplicity of notation we will henceforth take Λ_{ij} to denote the matrix of couplings *in the DM/quark mass-eigenstate basis*, and allow the spectrum of DM states to be arbitrary, with ϕ_1 being the lightest.

2.2. Decays of excited DM states

A priori we have three dark matter particles since ϕ_i is a triplet. As long as the mediators are heavier than the DM, the decay $\phi \to \chi q$ is forbidden and the Z_2 symmetry under which both ϕ and χ are charged guarantees the stability of ϕ_1. However, if there are mass splittings, as we generically expect there to be, then only the lightest state is stable, since a heavier one ϕ_2 can decay via $\phi_2 \to q_2 \bar{q}_1 \phi_1$. Even if the mass splitting is too small to produce the quarks, they can be virtual in a two-loop diagram to give $\phi_2 \to \phi_1 \gamma$, as shown in fig. 1. (In fact the photon must be off-shell since the effective operator $\partial_\mu \phi_2^* \partial_\nu \phi_1 F^{\mu\nu}$ vanishes for on-shell photons, but we can have for example $\phi_2 \to \phi_1 e^+ e^-$.)

3. LHC CONSTRAINTS ON MEDIATORS

The colored fermionic mediators of the model may be produced at the LHC, giving constraints on the mass of the new particle. Pair production of the mediator, with subsequent decay $\chi \to q\phi$, contributes to a signal characterized by final-state jets and missing transverse energy, denoted $\not{E}_T$. This is also the signature of squark and gluino production in the supersymmetric extension of the SM (SUSY). A recent ATLAS search for squarks and gluinos in this final state was presented in ref. [20].

Signals corresponding to different jet multiplicities are sensitive to the production of mediators that couple either to tops or to light quarks. A mediator that couples to light quarks has an identical signature to the light squark in SUSY, namely two jets and $\not{E}_T$. However, a colored fermion has a larger production cross section than a scalar. The signature of a t-coupled mediator is more similar to that of gluino production, having a final state with higher jet multiplicity; the decays of t and $\bar{t}$ in the

all-hadronic channel result in up to six jets.[1]

For this analysis, we simplify the model by ignoring the distinction between DM flavors (valid as long as their masses are much less than m_χ), and we allow for two mediators χ_u and χ_d. These can represent either the two components of the SU(2)-doublet χ in the Q model, or the SU(2)-singlet mediators of the u or d models. The interaction terms can then be written as

$$\lambda_{u_i}\,\phi\,\bar{\chi}_u P_{L(R)} u_i + \lambda_{d_i}\,\phi\,\bar{\chi}_d P_{L(R)} d_i + h.c. \qquad (4)$$

We used MadGraph5 [21] to calculate signal cross sections and to generate parton-level events. Implementation of the model in MadGraph is achieved with FeynRules [22].

The electroweak contributions to the mediator production cross section are highly subdominant to the QCD process. Fig. 2(a) shows the leading-order (LO) cross sections for the two subprocesses, verifying that the electroweak contributions may be neglected, as one would expect. The limits on χ_u and χ_d are thus equally applicable to the mediators of the u and d models, respectively.

We first consider the χ_d mediator. Ref. [20] provides an upper limit on the pair-production cross section for light squarks as a function of their mass. Under the assumption that the signal topology does not differ substantially for the mediator signal, we calculate the cross section for $\chi_d\bar{\chi}_d$ production and translate this limit to a 95 % c.l. bound on the mediator mass, applying a K-factor to account for higher-order corrections. The hadronic production mechanism of χ is the same as for any colored fermion: we therefore estimate the K-factor to be the same as for $t\bar{t}$ production, and obtain a value $K = 1.5$, comparing the NNLO value of the top pair-production cross section at $\sqrt{s} = 8$ TeV [23, 24] to the value calculated at LO. The limit is shown in fig. 2(b). We find that the mass of a down-coupled mediator is constrained to be $\gtrsim 920$ GeV, regardless of the coupling strength, as long as χ decays within the detector.

In the case of χ_u, the event topology of the signal may be substantially different than that from squark decays (other than $\tilde{t}$) due to the possible decay channel $\chi_u \to \phi\, t$. If this channel is suppressed, the signal is identical to that of χ_d, and the same limit $m_\chi \gtrsim 920$ GeV applies. A different approach is necessary for the $\chi_u \to \phi\, t$ channel. In this case we use the ATLAS upper limit on the visible cross section, defined as the product of (cross section) $\times$ (reconstruction efficiency) $\times$ (signal acceptance), in other words, an effective cross section for the number of signal events observed. To obtain a limit, we simulate full events with hadronization and detector simulation in order to determine the signal acceptance and reconstruction efficiency of the mediator signal. Details are provided in appendix A.

[1] Events with leptonic and semi-leptonic top-antitop decays are rejected in the analyses

The resulting limit on $\chi_u \to \phi\, t$, obtained from the 95% c.l. upper bound on the visible signal cross section, is shown in fig. 3. The exclusion region in the (m_{χ_u}, m_ϕ) plane is shown for the signal regions (SRs) with the highest sensitivity, and thereby the greatest exclusion reach. These correspond to SRs having four jets, with both loose and medium-level kinematic cuts (4jl and 4jm), the five-jet signal region (5j) in the case of 100% decays to top quarks, and the two-jet signal region, with medium-level cuts (2jm), for the other cases. For light DM, $m_\phi \lesssim 400$ GeV, the limit corresponds to a lower bound on a top-coupled mediator mass of ~ 1 TeV in the case of decays exclusively to tops. The bound relaxes with branching fraction to ~ 900 GeV; the exclusion by the 4j SR is relaxed, while that of the 2j SR becomes stricter, as the branching fraction to $t\phi$ is decreased.[2]

4. RELIC ABUNDANCE

Since our DM candidate is a complex scalar, its particle and antiparticle are distinct and it could therefore be an example of asymmetric dark matter, whose abundance arises through the generation of a particle-antiparticle asymmetry in the early universe. However, this would require a more complicated model, so we will assume that such an asymmetry is negligible and that the relic abundance comes from thermal freezeout of the annihilation processes. These can proceed either through t-channel exchange of the mediator χ or the $\lambda_{ij}\,\phi_i^*\phi_j|H|^2$ coupling, as shown in fig. 4. It will turn out that the former is the dominant process only in models with annihilation to top quarks, and with m_ϕ exceeding some minimum value to be determined. We consider χ-mediated annihilations first, and subsequently treat the Higgs portal scenario, constraining λ_{11} as a function of m_{ϕ_1} in order to get the observed abundance of dark matter.

4.1. Mediator dominance

We begin by evaluating the amplitude in fig. 4(a) for $\phi_i^*\phi_k \to q_l\bar{q}_j$. In general, the final-state quarks could be different from each other, and likewise the initial dark matter flavors could be distinct. To simplify the kinematics we will evaluate the cross section in the approximation that the DM mass splittings and quark masses are small compared to the average m_ϕ. At kinematic threshold, where the DM is at rest, the spin-summed,

[2] As the third-generation coupling is taken to zero, the limiting value of the lower bound on m_χ is slightly lower than in the light quark case, fig. 2(b). We adopt the latter constraint, as the discrepancy is most likely a result of using different simulation and reconstruction methods than those of ref. [20], as well as some subtler differences between the analyses.

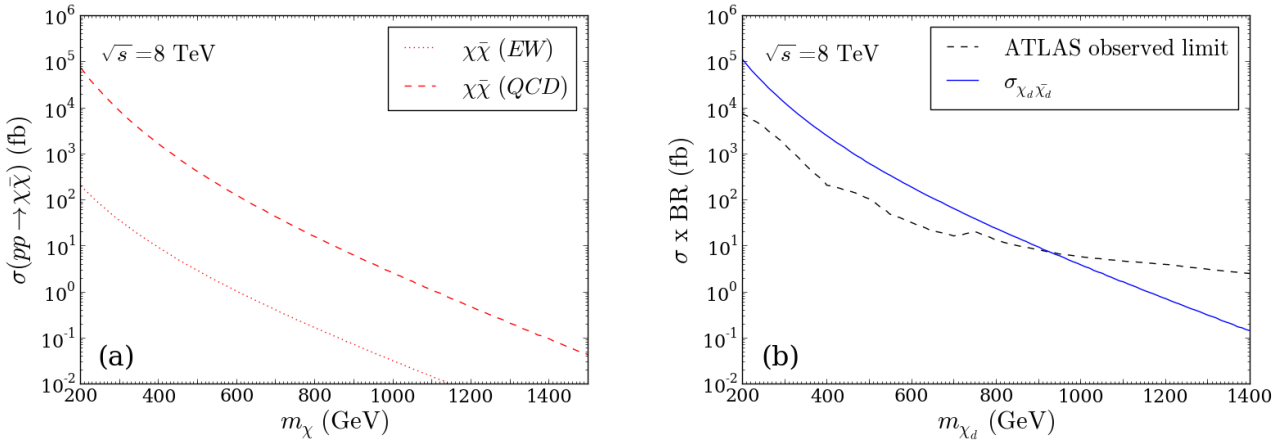

Figure 2: Left (a): comparison of the relative magnitudes of electroweak and QCD contributions to mediator production cross section at the LHC for c.m. energy $\sqrt{s} = 8$ TeV. Right (b): lower bound on the mass of a colored mediator coupling to light quarks, resulting from the upper limit on $\chi\bar{\chi}$ production cross section in final states with jets and $\not{E}_T$.

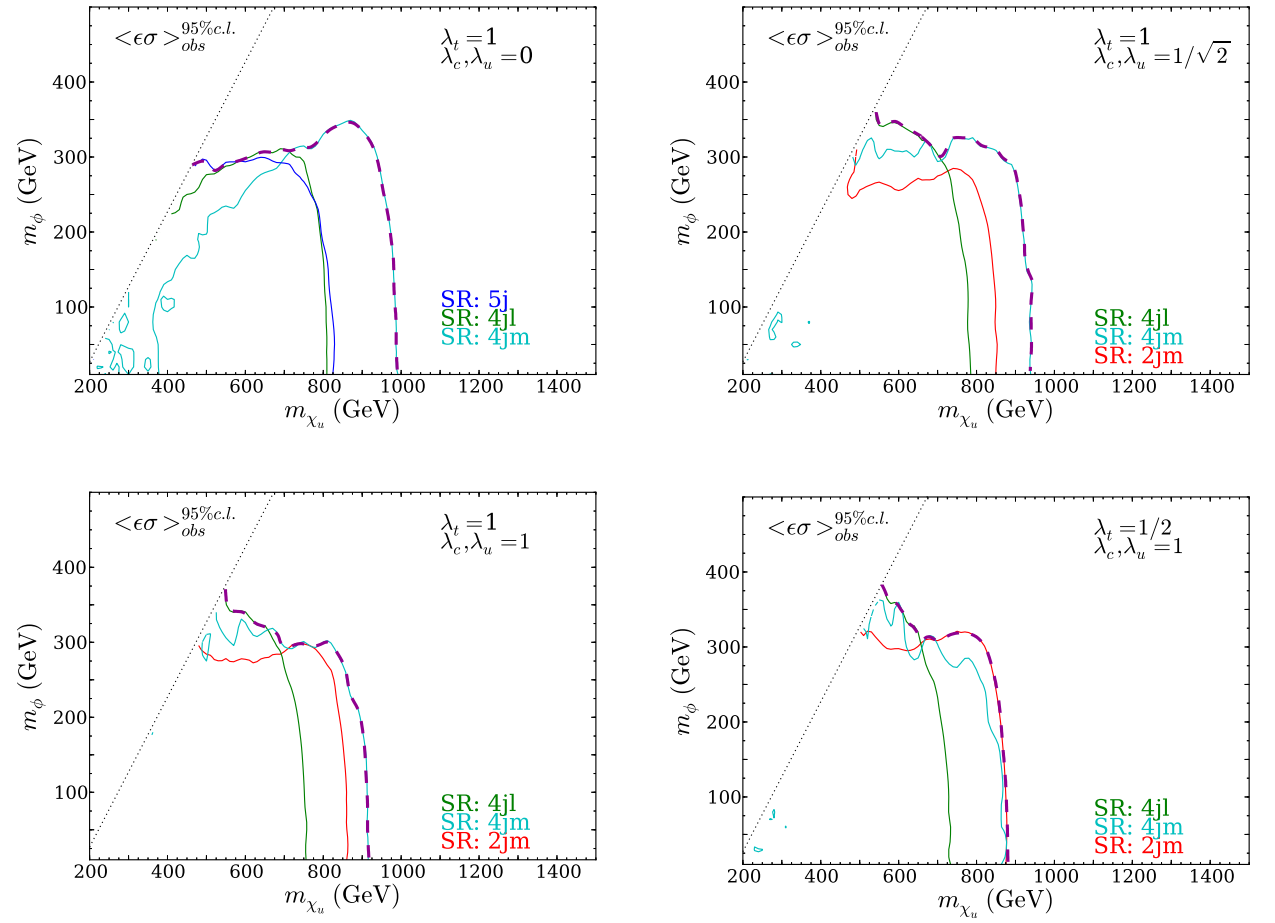

Figure 3: ATLAS constraints on DM mass versus up-type mediator mass for different branching fractions of $\chi \to \phi t$ (as opposed to decays into light quarks): BF = 1, 0.5, 0.3, and 0.1 from left to right and top to bottom. Regions below and to the left of the dashed curves (envelope of exclusion from signal regions with 2, 4 and 5 jets) are excluded.

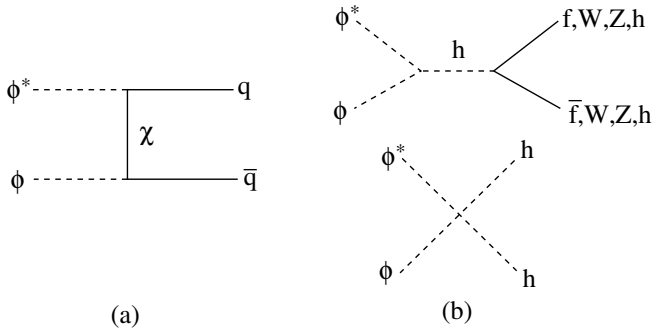

Figure 4: Processes contributing to thermal freezeout of scalar dark matter: (a) by exchange of the mediator χ; (b) through Higgs portal interactions. Possible decays of h in the lower diagram are not shown.

squared matrix element is

$$|\mathcal{M}|^2 = 6|\Lambda_{ij}\Lambda^*_{kl}|^2 \frac{m_q^2\,(m_\phi^2 - m_q^2)}{(m_\phi^2 + m_\chi^2 - m_q^2)^2}\ , \qquad (5)$$

including the sum over colors. The annihilation cross section is then given by

$$\sigma v_{\rm rel} = \frac{|\mathcal{M}|^2}{32\pi m_\phi^2}\sqrt{1-(m_q/m_\phi)^2}\ . \qquad (6)$$

To get the right relic density, we can match this to the value found in ref. [25], where the required cross section as a function of mass is derived. More specifically, for complex scalar DM, the required cross section is twice as large as that given in [25], where self-conjugate DM was assumed. Moreover, if the higher-mass DM states are in thermal equilibrium at the time of freeze-out, we must multiply the fiducial value of the cross section for a single complex scalar by the total number of complex DM components.

The result is shown in fig. 5(a), assuming a mediator mass of $m_\chi = 1$ TeV, and considering only the case where the final state is $t\bar{t}$, since for the lighter quarks, the suppression by m_q^2 leads to nonperturbatively large values of Λ_{ij}. Thus mediator exchange can only be the dominant contribution to annihilation in the Q and u models.

4.2. Higgs portal dominance

In the case where the Higgs portal interactions dominate the dark matter annihilation cross section, the required value of λ_{ij} can be deduced by rescaling with respect to real scalar singlet dark matter, which has been studied in detail in many references, including [26]. Since the abundance scales as $1/\langle\sigma v\rangle \sim 1/\lambda_{ij}^2$, we must increase λ_{ij} by a factor of $\sqrt{2}$ for complex ϕ relative to a real singlet, to compensate for the doubling of the number of degrees of freedom. In our model, there are actually three complex scalar dark matter states, because of the flavor multiplicity. If they are all degenerate, then λ_{ij} must be increased by a further factor of $\sqrt{2}^2$ relative to the complex singlet case. The exact value required will depend upon the mass splittings of the DM matter states and the thermal history. In particular, if the heavier DM states decay before freezeout, they will not contribute to the final abundance, whereas if they decay afterwards, they will. The range of possibilities is covered by the three curves shown in fig. 5(b).

4.3. When can mediators dominate?

In order to determine in which cases the Higgs portal interactions dominate over mediator exchange for setting the relic density, we note that the couplings λ_{ij} can naturally be no smaller than typical values generated by the loop diagrams shown in fig. 6. One could fine tune the bare value of λ_{ij} to cancel the loop contribution, but in the absence of such tuning one would expect a minimum magnitude for λ_{ij}, which we estimate by taking the leading logarithmic contribution and evaluating the log between the DM mass scale of order 100 GeV and a UV scale $\Lambda = 10$ TeV, which we take to be the minimum scale of validity for our model, considered as a low-energy effective theory. In this case, $\ln(\Lambda^2/m_\phi^2) \cong 9$, and by evaluating the loop we get the estimate

$$|\lambda_{ij}| \gtrsim \frac{27}{8\pi^2}(\Lambda y y^\dagger \Lambda^\dagger)_{ij} \cong \frac{27\,\Lambda_{i3}\Lambda^*_{j3}}{8\pi^2 v^2}\begin{cases} m_b^2, & y = y_d \\ m_t^2, & y = y_u \end{cases}\ , \qquad (7)$$

where Λ_{ij} is the $\phi\bar{\chi}q$ coupling and y_{ij} the Yukawa coupling relevant to the particular model of interest; $v = 174$ GeV is the complex Higgs VEV. Which Yukawa matrix appears depends upon the mediator. If the mediator is u- or d-like, then $y = y_u$ or y_d respectively. But if it is the doublet (Q-like), then we must sum over both possibilities, in which case y_u dominates. In either case, working in the basis of diagonal Yukawa matrices gives the approximation shown in (7).

By substituting the value of $|\Lambda_{ij}|$ shown in fig. 5(a) into eq. (7), and comparing to the value of λ_{ij} shown in fig. 5(b), we can determine when it would be inconsistent to assume that mediator exchange dominates over Higgs portal interactions. This comparison is shown in fig. 7, for models where y_u rather than y_d appears in the loop (otherwise, the solid curve is lower by a factor of $(m_b/m_t)^2$, giving no useful constraint). We assumed for these curves that only one DM flavor is in equilibrium; for higher numbers, both curves scale upward by the same factor, so that the values of m_ϕ where they intersect do not change.

It is interesting to notice that the same model-building choices that would suppress the loop contribution (7) also suppress the mediator contribution to annihilation. In particular, the models for which $y = y_d$ in (7) are those where the mediator is d-like, but these have cross sections for $\phi\phi \to q\bar{q}$ suppressed at least by m_b^2 in eq. (5), making

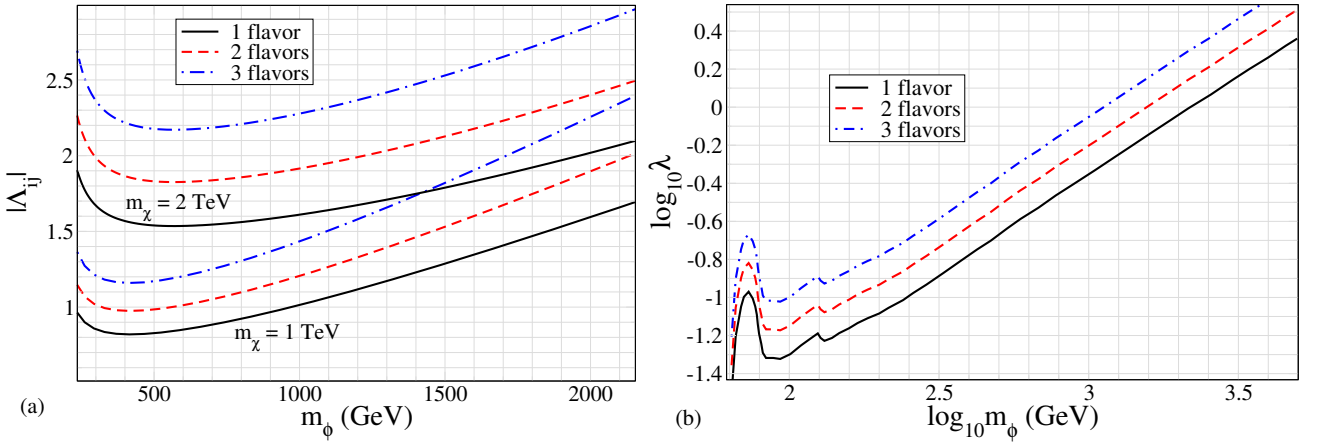

Figure 5: Left (a): value of DM-mediator-quark coupling $|\Lambda_{ij}|$ needed for thermal relic abundance from annihilations via t-channel mediator exchange, as a function of DM mass m_ϕ, assuming $\phi^*\phi \to t\bar{t}$ and $m_\chi = 1$ TeV (lower curves) or $m_\chi = 2$ TeV (upper curves). Different curves show the dependence upon how many flavors of DM are in equilibrium at the time of freezeout. Right (b): value of DM-Higgs cross coupling needed for thermal relic abundance from Higgs portal annihilations, again showing the dependence on number of DM flavors in equilibrium at freezeout.

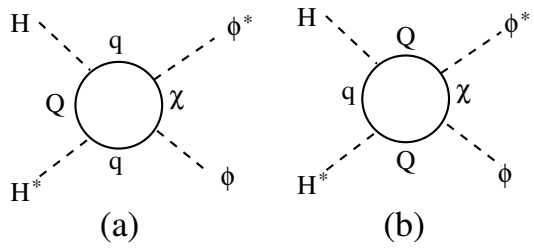

Figure 6: One-loop contribution to $\lambda_{ij}\phi_i^*\phi_j|H|^2$ interaction, where $q\,(Q)$ stands for electroweak singlet (doublet) quarks, and the routing of weak isospin is shown for (a) singlet and (b) doublet mediators, respectively.

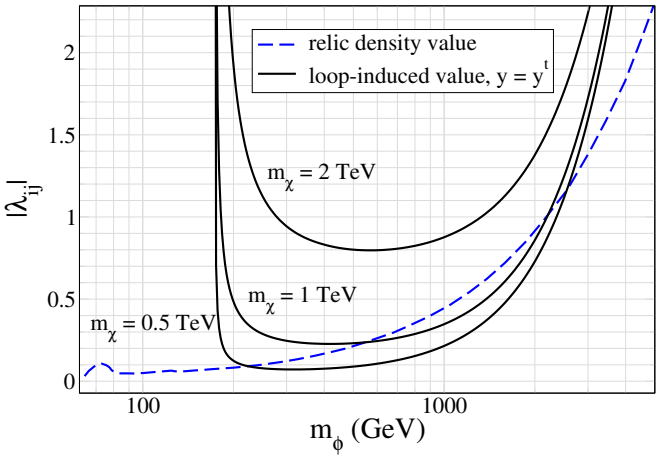

Figure 7: Comparison of the value of $|\lambda_{ij}|$ needed for correct relic density via Higgs portal annihilations (dashed curve) with the value coming from loop contributions, eq. (7), in the case where $|\Lambda_{ij}|$ is large enough for mediator exchange to give the right relic density (also assuming that y_u rather than y_d is the Yukawa coupling matrix appearing in the loop). Models where the solid curve is higher than the dashed one have annihilations dominated by the Higgs portal, in the absence of fine tuning.

it impossible to satisfy the relic density constraint with reasonable values of Λ_{ij}.

The upshot of this analysis is that only in the Q and u models with 300 GeV $\lesssim m_\phi < m_\chi$ and $m_\chi \cong$ 0.5-1 TeV can we consistently assume mediator dominance of the annihilation cross section. Here we have taken advantage of the fact that our LHC constraint on m_χ is weaker for $m_\phi \sim 300$ GeV than for lighter m_ϕ; see fig. 3 (upper left). Moreover, the tree-level value of λ_{ij} can exceed the minimum coming from the loop estimate in eq. (7); thus Higgs portal dominance is always a logical possibility, even when not a necessity.

5. INDIRECT DETECTION

Annihilation of DM in our galaxy or neighboring ones can produce gamma rays from the decays of final-state particles. The Fermi Large Area Telescope (LAT) continues to improve constraints on dark matter annihilation into various final states, from observations of dwarf spheroidal galaxies that are relatively uncontaminated by baryonic background signals [27]. The constraints are strongest for light dark matter, whose relic density is higher. They are therefore relevant in the region of parameter space where annihilation is primarily through the Higgs portal.

For m_ϕ below the W/Z threshold, annihilation is almost exclusively into $b\bar{b}$. We reproduce the Fermi limit from ref. [27] on the annihilation cross section into $b\bar{b}$ in fig. 8(a), where it is relaxed by a factor of 2 due to the dark matter not being self-conjugate in our model. The

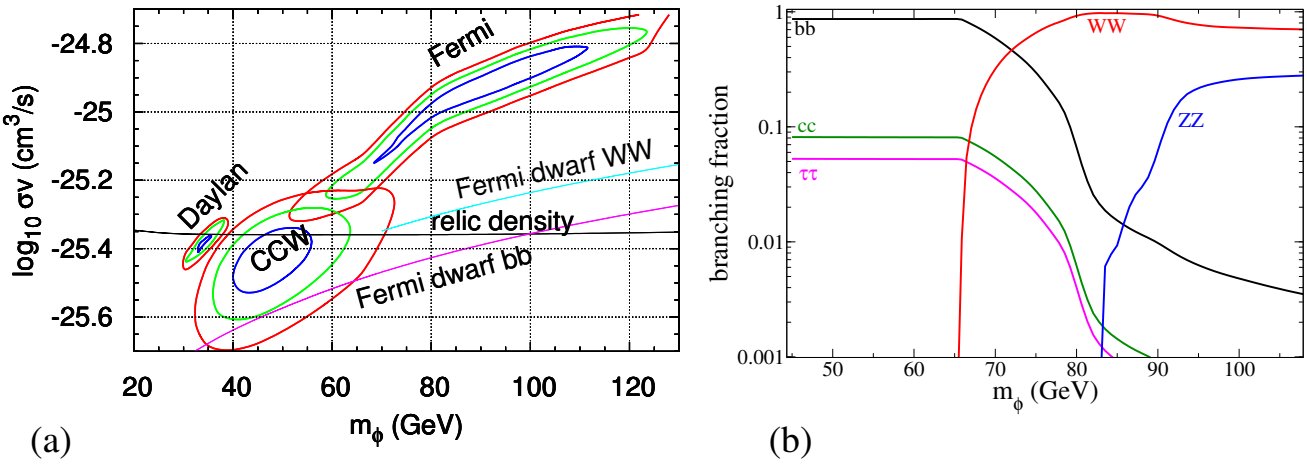

Figure 8: Left (a): cross section for $\phi^*\phi$ to annihilate through the Higgs portal, for relic density, galactic center gamma ray excess (1, 2 and 3σ contours for three data sets: Daylan *et al.*, CCW and Fermi), and Fermi/LAT upper limit from dwarf spheroidal galaxies assuming $b\bar{b}$ or WW final states. Right (b): branching fractions for $\phi^*\phi$ to annihilate into SM final states through the Higgs portal (adapted from ref. [26]).

value needed for the observed relic density (also increased by the factor of 2) is also shown, suggesting that masses below 100 GeV are ruled out. However, for $m_\phi > 70$ GeV, the dominant annihilation channel is no longer $b\bar{b}$ but rather WW or WW^* where one of the W's is off shell; fig. 8(b) shows the branching fractions into different final states. The constraint on the $WW + WW^*$ channel is weaker by a factor 1.3, which can allow for somewhat lighter dark matter ($m_\phi \sim 80$ GeV) to be consistent with both relic density and indirect constraints. The actual constraint on Higgs portal models (not determined by ref. [27]) interpolates between the WW and $b\bar{b}$ curves in the region $m_\phi = 70$-80 GeV.

5.1. Galactic center γ-ray excess

A possible signal in Fermi/LAT data for dark matter annihilation in the galactic center has been discussed by several groups, most recently in refs. [15–17] (referred to here as Daylan *et al.*, CCW and Fermi respectively). The Fermi collaboration itself presented preliminary evidence for gamma rays in excess of those attributable to known astrophysical sources in the central $15^\circ \times 15^\circ$ region of the galaxy [17, 28]. Recently, new evidence has been presented in favor of unresolved millisecond pulsars as a likely astrophysical source [28–31], but pending a definite resolution, it is interesting to explore whether dark matter models can consistently explain the observations.

Here we have used a similar methodology as in ref. [32] to fit m_ϕ and its annihilation cross section $\langle\sigma v\rangle$ to the excess signal as characterized respectively by Daylan *et al.*, CCW and Fermi. To generate the predicted signal, we compute the photon spectrum from annihilation into SM states with the branching ratios shown in fig. 8(b), using spectra from ref. [33]. These are compared to the data to compute χ^2 statistics for which the 1, 2 and 3σ-allowed regions are shown in fig. 8(a).

The three data sets are not fully consistent with one another, and they conflict with the Fermi dwarf constraint except for part of the CCW 3σ region. This region however has too small an annihilation cross section with respect to that needed for the relic density, by a factor of $\cong 1.2$, which would lead to a 20% increase in the dark matter abundance. The experimental error in the observed abundance as determined by Planck is about 4%. A consistent interpretation would require that the actual excess signal be somewhat lower in intensity, as may be the case if part of it is due to millisecond pulsars.

6. DIRECT DETECTION

Our dark matter candidate can scatter elastically with quarks through mediator exchange, fig. 9(a), leading to DM-nucleon scattering that is constrained by direct detection experiments. This can occur either by the coupling of ϕ to valence quarks, or that to heavy quarks via the loop diagram fig. 9(b) that enables photon exchange. In addition, the Higgs portal coupling allows for $\phi N \to \phi N$ scattering by Higgs boson exchange. For DM masses $m_\phi \gtrsim 6$ GeV, the strongest current limits come from the LUX experiment [34]. We will first derive constraints on the different kinds of interactions assuming that they do not interfere with each other significantly. In section 6.3 we will consider the possibility of destruc-

tive interference that could weaken direct detection constraints sufficiently to allow for the indirect signals we discussed in section 5.

6.1. Mediator-induced interactions

We first consider the nonelectromagnetic mediator-induced interaction. It is straightforward to show that fig. 9(a) leads to an effective operator[3]

$$\frac{|\Lambda_{1i}|^2}{m_\chi^2}(\phi^*\partial_\mu\phi)\,(\bar{q}_i\gamma^\mu P_{L,R}\,q_i)\ , \tag{8}$$

where the sum over doublet components is taken in the Q model. When taking matrix elements of this operator between nucleon states, the only nonvanishing contributions are from the valence quarks $i = u, d$, giving the cross section [35]

$$\sigma_{p,n} = \frac{\mu^2\, f_{p,n}^2}{4\pi m_\phi^2} \tag{9}$$

for scattering of ϕ on protons or neutrons, where μ is the ϕ-nucleon reduced mass and $f_{p,n} = |\Lambda_{1i}|^2/m_\chi$, up to isospin-related factors of order unity, depending upon which DM model we are considering.[4] The LUX constraint on these couplings is shown in fig. 10(a) for mediator mass $m_\chi = 1$ TeV. The limit on Λ_{13} is orders of magnitude smaller than values of interest for the relic density for the coupling to top quarks. There must be a large generational hierarchy in the couplings Λ_{1i}, at least between the first and higher generations.

Next we consider the contribution from the penguin diagram, fig. 9(b). The loop leads to the effective photon-DM interaction

$$\frac{\kappa\, e}{m_\chi^2 - m_\phi^2}\,(\phi^* \overleftrightarrow{\partial_\mu}\phi)\,\partial_\nu F^{\mu\nu}\ . \tag{10}$$

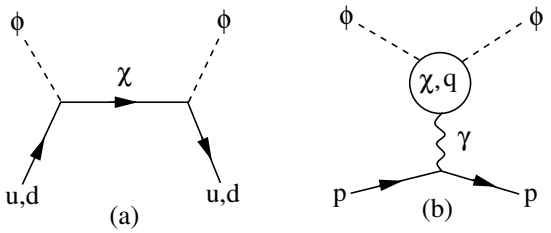

Figure 9: SFDM contributions to ϕ-nucleon scattering via the $\phi\bar{\chi}q$ interaction: (a) tree-level mediator exchange, and (b) penguin diagram for DM-proton interaction.

[3] Here we ignore contributions suppressed by m_q that are irrelevant for ϕ-nucleon scattering.

[4] For f_p these factors are (1, 1/2, 3/2) for the u, d, Q models, while for f_n they are (1/2, 1, 3/2), respectively.

For the three models (u, d, Q), κ is approximately given by

$$\kappa \cong \frac{1}{16\pi^2}\begin{cases} Q_q \sum_i |\Lambda_{1i}|^2 \ln\left(\frac{m_{q_i}^2}{m_\chi^2}\right), & q = u \text{ or } d \\ \sum_{q,i} Q_q |\Lambda_{1i}|^2 \ln\left(\frac{m_{q_i}^2}{m_\chi^2}\right), & Q \text{ model} \end{cases} \tag{11}$$

in the limit $m_\phi \ll m_\chi$, where $Q_q = 2/3$ or $-1/3$ is the charge of the quark and m_{q_i} is its mass. For larger m_ϕ, the loop integral depends differently upon m_ϕ, and the logarithm gets replaced by

$$\frac{1}{(m_\chi^2 - m_\phi^2)}\ln\left(\frac{m_{q_i}^2}{m_\chi^2}\right) \to \frac{1}{m_\chi^2} I(\epsilon, \epsilon_i)\ , \tag{12}$$

where we define $\epsilon_\phi = m_\phi^2/m_\chi^2$, $\epsilon_i = m_{q_i}^2/m_\chi^2$, $D(x) = x + \epsilon_i(1-x) - \epsilon_\phi x(1-x)$, $D'(x) = D(1-x)$ and

$$\begin{aligned} I \ &= \ \int_0^1 dx \left[(1-x)^3(1+2x)\left(\frac{1}{D'} - \frac{1}{D}\right)\right. \\ &+ \ \left.(1-x)^4\left(\frac{\epsilon_i + \epsilon_\phi x^2}{2D^2} - \frac{1+\epsilon_\phi x^2}{2D'^2}\right)\right]. \end{aligned} \tag{13}$$

The large logarithm comes from $1/D$ as $x \to 0$.

The resulting photon-mediated DM-proton scattering cross section is given by

$$\sigma_p \ = \ \frac{16\pi\,\mu^2\alpha^2\kappa^2}{(m_\chi^2 - m_\phi^2)^2}\ , \tag{14}$$

where μ is the ϕ-proton reduced mass. The limits from this process are much weaker than those from the nonelectromagnetic coupling. Also, whereas that one bounded only Λ_{11}, this one applies to Λ_{1i} for all the quark generations. Hence we take $i = 2, 3$, (recall that $i = 3$ represents the couplings relevant for the relic density in section 4.1). Ignoring possible interference between different generations, we obtain the limits shown in fig. 10(b), with solid (dashed) curves corresponding to $i = 3(2)$. These couplings are somewhat weaker than the values leading to the right relic density in fig. 5(a).

6.2. Higgs portal interaction

For the Higgs portal coupling, the effective DM-nucleon scattering cross section is given in ref. [26]:

$$\sigma \ = \ \frac{\lambda_{11}^2 f_N^2}{4\pi}\frac{\mu^2 m_p^2}{m_H^4 m_\phi^2}\ , \tag{15}$$

where $f_N = 0.303$ [26] is related to the Higgs-nucleon coupling, and $m_H = 125$ GeV. The LUX data can be used to put limits on the the coupling λ_{11}, as shown in Fig. 11. The value of λ_{11} needed for the observed relic density is also plotted, for the case where only ϕ_1 is

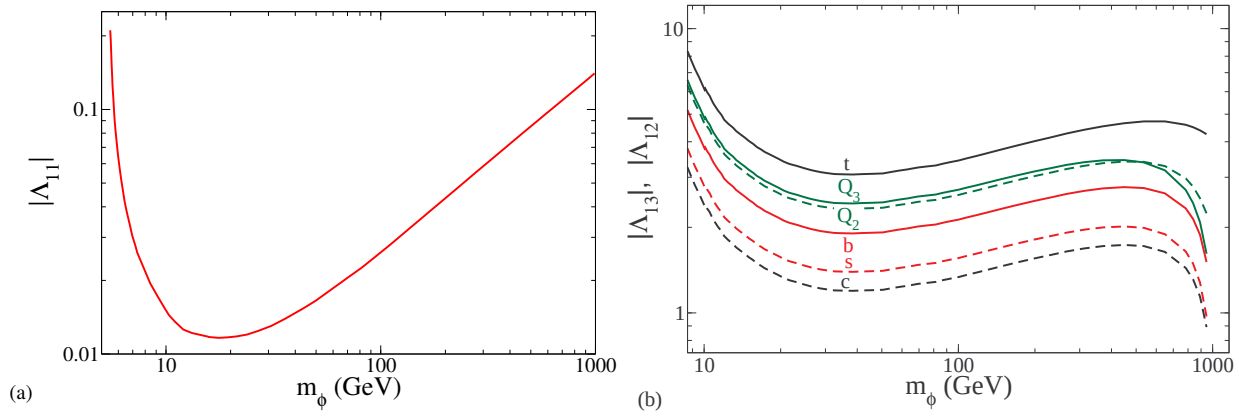

Figure 10: Left (a): LUX constraints on the coupling of dark matter to light quarks u, d, assuming mediator mass $m_\chi = 1$ TeV. Right (b): LUX constraints on couplings between Λ_{13} (solid curves) and Λ_{12} (dashed curves), for different choices of the quark appearing in the loop of fig. 9(b), depending upon the choice of model (d, u or Q). The mediator mass is assumed to be $m_\chi = 1$.

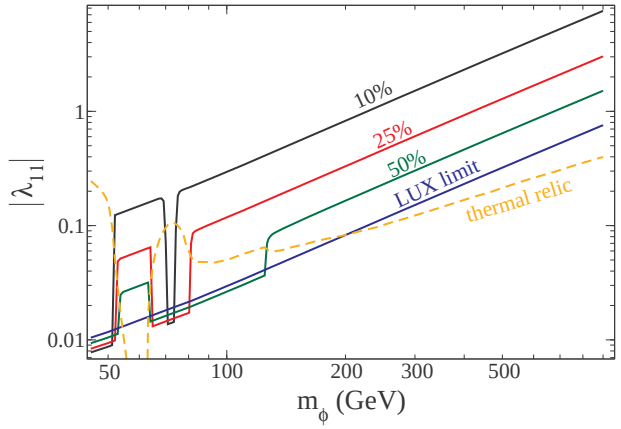

Figure 11: Solid curves: LUX and relic density constraints on the Higgs portal coupling λ_{11}, taking dark matter to be asymmetric and accounting for accidental cancellation at the level of 100, 50, 25 and 10% by the mediator contribution to the scattering amplitude. 100% means no cancellation, giving the usual exclusion curve. Dashed curve: value of λ_{11} that would give thermal relic abundance.

relevant during freeze-out. The LUX limit must lie below the relic density curve if the DM has a thermal origin. In addition to the allowed range $m_\phi \gtrsim 150$ GeV, there is a narrow window of lower masses for which the relic density is not exceeded around $m_\phi \cong m_h/2$, corresponding to resonantly-enhanced annihilations.

6.3. Higgs-mediator interference

Fig. 11 shows that the interesting DM mass range for indirect detection (fig. 8) is ostensibly ruled out by the LUX limit. However, we have not yet taken into account the possibility of destructive interference between different contributions to the ϕ-nucleon scattering amplitude. This is clearly possible for either dark matter particles or their antiparticles, since the effective operator (8) changes sign under charge conjugation of ϕ while the amplitude from Higgs exchange does not. Since eqs. (9) and (15) have the same dependence upon m_ϕ, it is particularly simple to combine them taking account of interference:

$$\sigma_n \cong \left(\lambda_{11} f_N \frac{m_p}{m_h^2} \pm \frac{|\Lambda_{11}|^2}{m_\chi}\right)^2 \frac{\mu^2}{4\pi m_\phi^2} \,. \qquad (16)$$

If interference is destructive for ϕ it will be constructive for ϕ^*. Therefore to have a net reduction, it is necessary to consider asymmetric dark matter where the antiparticle abundance is suppressed [36]. The suppression factor has been computed as a function $r(\lambda/\lambda_0) = n_{\phi^*}/n_\phi$ (the ratio of anti-DM to DM) in ref. [37], where λ_0 denotes the value of the coupling that would give rise to the correct thermal relic abundance.[5] If the amplitude for scattering of DM on nucleons is reduced by the factor $(1-\epsilon)$, and that for anti-DM is increased by $(1+\epsilon)$, and the nominal bound is $\lambda_{\rm LUX}$, then the relaxed bound on the coupling is given by

$$\lambda_{\rm eff} = \frac{\lambda_{\rm LUX}}{[(1-\epsilon)^2(1-r/2) + (r/2)(1+\epsilon)^2]^{1/2}} \qquad (17)$$

where $r = r(\lambda_{\rm eff}/\lambda_0)$. Eq. (17) gives only an implicit definition of $\lambda_{\rm eff}$, but it can be solved numerically by iteration.

In fig. 11 we show the modified upper limits on $|\lambda_{11}|$ that result from allowing for accidental cancellations that

[5] Denoting $x = (\lambda/\lambda_0)^2$, we are able to fit the numerical result of ref. [37] to the function $-\log_{10} r = (A_0 x + A_1)/(1 + A_2 x^{A_3})$, where $A_0 = 0.8327$, $A_1 = -0.8258$, $A_2 = -0.8737$, $A_3 = -0.8213$, which is valid for $x \geq 1$. For $x < 1$, $r = 1$.

reduce the amplitude to 75%, 50% and 10% of its magnitude in the absence of the mediator contribution. It is clear that the range of allowed masses can be considerably widened relative to the thermal abundance scenario.

The mediator diagram can have a significant effect only for ϕ-nucleon scattering, and not $\phi\phi^*$ annihilation, because of the quark vector current in the effective interaction (8). Its matrix element for $\phi\phi^* \to q\bar{q}$ is suppressed by $m_q = m_b$ for the mass range of interest, while that for $\phi N \to \phi N$ suffers from no such kinematic reduction.

7. DM-INDUCED FLAVOR EFFECTS

We now turn to the implications of scalar flavored dark matter for particle-physics phenomenology, including FCNC processes, rare decays, and CP violation. We recall our choice of the underlying flavor symmetry group as $\mathrm{SU}(3)_\phi \times \mathrm{SU}(3)_Q \times \mathrm{SU}(3)_u \times \mathrm{SU}(3)_d$ [19], which is broken by the SM Yukawa couplings and our new couplings Λ_{ij}. Because the mediator χ is forced to be heavy by LHC constraints, we do not need to rely upon a more restrictive flavor structure such as MFV [18] to keep flavor-changing neutral currents under control, as will become clear in this section. However, we will demonstrate the potential of the model to give rise to observable low-energy effects for values of the couplings Λ_{ij} that are consistent with the constraints obtained in the previous sections.

7.1. Flavor-changing meson oscillations

We briefly review the formalism for $\Delta F = 2$ flavor-changing oscillations of neutral mesons. To be concrete, we illustrate this for the case of $\Delta B = 2$ meson mixing. In the B^0-$\bar{B}^0$ basis, the mixing is described by the 2×2 matrix $M - \frac{i}{2}\Gamma$, in which the mass (M) and decay (Γ) matrices are Hermitian. The physical states are [38]

$$\begin{aligned} |B_L\rangle &= p\,|B^0\rangle + q\,|\bar{B}^0\rangle \ , \\ |B_H\rangle &= p\,|B^0\rangle - q\,|\bar{B}^0\rangle \ , \end{aligned} \tag{18}$$

with eigenvalues ($L =$ "light," $H =$ "heavy")

$$\mu_{L,H} = M_{L,H} - \frac{i}{2}\Gamma_{L,H} \ , \tag{19}$$

in which $M_{L,H}$ and $\Gamma_{L,H}$ denote the masses and decay widths of $B_{L,H}$. In addition,

$$\frac{q}{p} = \pm \left(\frac{M_{12}^* - i\Gamma_{12}^*/2}{M_{12} - i\Gamma_{12}/2} \right)^{1/2} \ . \tag{20}$$

It is a good approximation to take $|\Gamma_{12}| \ll |M_{12}|$; then

$$\Delta M \equiv M_H - M_L \cong 2\,|M_{12}| \, . \tag{21}$$

In our model, the matrix element M_{12} receives new contributions beyond the SM from box diagrams with ϕ and χ in the loop.

7.1.1. B_s^0-$\bar{B}_s^0$ mixing

The DM-induced contributions to B_s^0-$\bar{B}_s^0$ mixing from box diagrams with ϕ and χ in the loop can be described by the effective operator [19]

$$\frac{(\Lambda^\dagger \Lambda)_{bs}^2}{128\pi^2\, m_\chi^2} \left(\bar{b}\, \gamma^\mu P_{L,R}\, s \right)^2 \tag{22}$$

in the Q- (P_L) and d-type (P_R) models, where we used the approximation $m_{\phi_i} \ll m_\chi$.[6] The corresponding mass splitting is $(\Delta M_s)_{DM} = |(\Lambda^\dagger\Lambda)_{bs}^2| m_{B_s} f_{B_s}^2/(192\pi^2\, m_\chi^2)$. The measured value is $(\Delta M_s)_{\rm exp.} = (11.69 \pm 0.02) \times 10^{-9}$ MeV, while the SM prediction is $(\Delta M_s)_{\rm SM} = (11.4 \pm 1.7) \times 10^{-9}$ MeV [39]. These quantities are related via

$$(\Delta M_s)_{\rm exp.} = 2\,|(M_{12})_{\rm SM} + (M_{12})_{\rm DM}| \ . \tag{23}$$

To obtain constraints on the DM contribution to (23), one has to take into account a possible phase difference between $(M_{12})_{\rm SM}$ and $(M_{12})_{\rm DM}$. But this phase difference will also manifest itself in q/p, eq. (20). A rigorous analysis would require a simultaneous fit to the measured values of ΔM_s and $\arg(q/p)$, which is beyond the scope of this paper. Instead, to estimate the allowed size of the new contribution, we neglect any phase difference, leading to $|\Delta M_s|_{\rm DM} = (0.3 \pm 1.7) \times 10^{-9}$ MeV, or $|\Delta M_s|_{\rm DM} \le 5.4 \times 10^{-9}$ MeV at 3σ. For $m_\chi = 1$ TeV, this corresponds to the limit $|(\Lambda^\dagger\Lambda)_{bs}| < 0.19$. This is smaller than the direct detection bounds on second-generation couplings shown in fig. 10(b).

As can be seen from the above values of $(\Delta M_s)_{\rm exp.}$ and $(\Delta M_s)_{\rm SM}$, the measurement of B_s-$\bar{B}_s$ mixing is consistent with the SM prediction. On the other hand, the theoretical error on this prediction is sizeable, leaving ample room for a new-physics contribution to ΔM_s. Indeed, if $|\Delta M_s|_{\rm DM}$ saturates its upper limit, it will be of the same order as $|(\Delta M_s)_{\rm SM}|$. We therefore see that flavored DM could contribute significantly to B_s-$\bar{B}_s$ mixing with reasonable values of the couplings.

7.1.2. K^0-$\bar{K}^0$, D^0-$\bar{D}^0$, B_d^0-$\bar{B}_d^0$ mixing

A similar analysis can be done for oscillations of the other neutral meson systems, K^0-$\bar{K}^0$, D^0-$\bar{D}^0$, B_d^0-$\bar{B}_d^0$. Constraints on the coefficients c_{ij} of the effective operator $\Lambda^{-2}(\bar{q}_i \gamma_\mu P_L q_i)^2$ (where Λ is the new physics scale) have been compiled for example in ref. [40]. These can be related to the prediction (22), with appropriate substitution of quark flavors. The results are shown in table I. For K^0-$\bar{K}^0$ and D^0-$\bar{D}^0$ mixing, we obtain separate

[6] This follows from eq. (4.1) of ref. [19], accounting for the loop now being dominated by momenta of order m_χ, and ignoring corrections of order $(m_\phi/m_\chi)^2$.

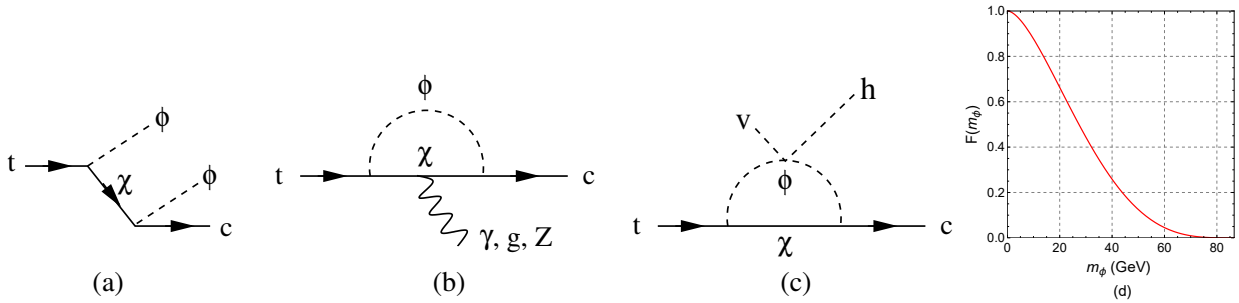

Figure 12: Diagrams for (a) $t \to \phi\phi^* c$, (b) $t \to c\gamma$ or other gauge bosons, (c) $t \to hc$, and (d) the function $F(m_\phi)$ determining the partial width for $t \to \phi\phi^* c$ relative to its maximum value.

ij	$\mathrm{Re}[(\Lambda\Lambda^\dagger)^2_{ij}]$	$\mathrm{Im}[(\Lambda\Lambda^\dagger)^2_{ij}]$
ds	1.1×10^{-3}	4.3×10^{-6}
uc	7.1×10^{-4}	1.3×10^{-4}
bd	3.6×10^{-4}	
bs	8.3×10^{-3}	

Table I: Bounds on FCNC matrix elements of $(\Lambda\Lambda^\dagger)_{ij}$ with $i \neq j$ from neutral meson mixing, assuming mediator mass $m_\chi = 1\,\mathrm{TeV}$. Values for the first two rows are inferred using constraints reported in ref. [40]. For $B_{d,s}$ (last two rows) we constrain only the modulus $|(\Lambda\Lambda^\dagger)^2_{ij}|$ using updated experimental and SM fit numbers from [41].

constraints on the real and imaginary parts of $(\Lambda\Lambda^\dagger)^2_{ij}$ ($ij = ds, uc$). For B^0_d-$\bar{B}^0_d$ and B^0_s-$\bar{B}^0_s$ mixing, the constraints are given only for $|(\Lambda\Lambda^\dagger)^2_{ij}|$ ($ij = bd, bs$). The imaginary parts of $(\Lambda\Lambda^\dagger)^2_{ij}$ can lead to CP-violating effects, as we will discuss in section 7.4.

7.2. Flavor-changing top quark decays

SFDM allows for a variety of rare FCNC decays, including $t \to c(u)\phi\phi$ (if m_ϕ is sufficiently small), $b \to s\gamma$, $t \to (Z, h, g, \gamma)c$, and $(h, Z) \to b\bar{s}$. A summary of the Fermilab and LHC constraints on these processes is given in ref. [42]. With the exception of $t \to c\phi\phi$, these are unobservably small, despite having no symmetry (MFV) to suppress them. This is a consequence of the chiral structure of the interaction (1), which causes all amplitudes to be suppressed by $1/m^2_\chi$ and not just $1/m_\chi$.

If $m_\phi \lesssim m_t/2$, the tree-level processes $t \to c\phi\phi$ or $t \to u\phi\phi$ are allowed (fig. 12(a)). For the $c\phi\phi$ final state, the partial width is

$$\begin{aligned} \delta\Gamma &\cong \frac{(\Lambda^\dagger\Lambda)_{tt}(\Lambda^\dagger\Lambda)_{cc}\, m_t^5}{4096\,\pi^3\, m_\chi^4} F(m_\phi) \\ &= 2 \times 10^{-6}\,\mathrm{GeV} \cdot |\Lambda|^2_{tt}|\Lambda|^2_{cc}\, F(m_\phi)\ , \end{aligned} \tag{24}$$

where the dependence on m_ϕ is shown in fig. 12(d) and for the numerical estimate we took $m_\chi = 900$ GeV. The analogous formula with $c \to u$ applies for $t \to u\phi\phi$, but because of the more stringent constraint on first-generation couplings from direct detection, this is expected to be subdominant. With large couplings $\Lambda \sim 3$ and light DM with $m_\phi \sim 30\,\mathrm{GeV}$, eq. (24) would lead to a branching ratio of 3×10^{-5}. Recent studies of this process in other models with flavor-changing scalar DM coupling to the top estimate that LHC searches could ultimately be sensitive to such a small branching ratio [43–45]. Although our choice of m_ϕ is ruled out by direct detection for a thermally produced WIMP, since ϕ has a conserved particle number, there could be a DM asymmetry allowing for sufficiently small coupling to the Higgs for consistency with direct searches.[7]

A second class of decays is $t \to c +$ gauge boson, shown in fig. 12(b). ATLAS obtains upper limits of 1.7×10^{-4} on the branching ratio for $t \to cg$ and 4×10^{-5} for $t \to ug$ [46, 47]. Writing the NP contribution to the $t \to c$ chromomagnetic dipole moment as

$$g_s\, \kappa_{tcg}\, (\bar{t}\, \sigma^{\mu\nu} T^a P_{L,R}\, c)\, G^a_{\mu\nu} + \mathrm{h.c.}\ , \tag{25}$$

the limit on the branching ratio corresponds to $\kappa_{tcg} < 1.3 \times 10^{-2}\ \mathrm{TeV}^{-1}$. In our model

$$\kappa_{tcg} = (\Lambda^\dagger\Lambda)_{tc}\, \frac{m_t}{64\pi^2 m^2_\chi}\ , \tag{26}$$

implying the weak constraint $(\Lambda^\dagger\Lambda)_{tc} < 40$.

For the electromagnetic FCNC $t \to u\gamma$ decays, CMS finds a limit of 1.6×10^{-4} (1.8×10^{-3} for $t \to c\gamma$) [48]. This corresponds to a limit on the magnetic moment coefficient $\kappa_{tu\gamma}$

$$\frac{2e}{3}\, \kappa_{tu\gamma}\, (\bar{t}\, \sigma^{\mu\nu} P_{L,R}\, u)\, F_{\mu\nu} + \mathrm{h.c.} \tag{27}$$

of $\kappa_{tu\gamma} < 0.16\,\mathrm{TeV}^{-1}$, and a correspondingly weaker limit of $(\Lambda^\dagger\Lambda)_{tu} < 580$. The best limit on $t \to qZ$ also comes from CMS, with an upper bound of $\mathrm{BR} < 5 \times 10^{-4}$ [49], leading to $(\Lambda^\dagger\Lambda)_{tc} + (\Lambda^\dagger\Lambda)_{tu} \lesssim 785$ for models with Q-like mediators, and somewhat less stringent for u-like.

[7] This would also require some fine tuning of the loop contributions to λ_{ij}, according to the considerations of section 4.3.

The decay mode $t \to ch$ shown in fig. 12(c) has a partial width of order

$$\delta\Gamma \cong \left(\frac{v(\Lambda^\dagger\lambda\Lambda)_{tc}}{16\pi^2\, m_\chi^2}\right)^2 \frac{m_t(m_t^2 - m_h^2)}{16\pi} \cong 2\times 10^{-7}(\Lambda^\dagger\lambda\Lambda)_{tc}^2\,\mathrm{GeV}\ , \quad (28)$$

which is far below the current sensitivity of $\delta\Gamma \lesssim 1\,\mathrm{GeV}$ [50] for reasonable value of the couplings.

7.3. Flavor-changing b decays

The radiative flavor-changing processes $b \to s\gamma$ and $b \to s\ell^+\ell^-$ are described by the effective operators

$$\mathcal{O}_7 = \frac{e}{(4\pi)^2} m_b(\bar{s}\sigma^{\mu\nu}P_R b)F_{\mu\nu}\ ,$$
$$\mathcal{O}_9 = \frac{e^2}{(4\pi)^2}(\bar{s}\gamma_\mu P_L b)(\bar{\ell}\gamma^\mu \ell)\ ,$$
$$\mathcal{O}_{10} = \frac{e^2}{(4\pi)^2}(\bar{s}\gamma_\mu P_L b)(\bar{\ell}\gamma^\mu\gamma_5 \ell) \quad (29)$$

and their chirality-flipped counterparts, $\mathcal{O}'_7$, $\mathcal{O}'_9$ and $\mathcal{O}'_{10}$, obtained by taking $P_L \leftrightarrow P_R$. The operators $\mathcal{O}_{7,9,10}$ are induced by the Q model, while the d model generates $\mathcal{O}'_{7,9,10}$.

7.3.1. $b \to s\gamma$

The decay $b \to s\gamma$ has reduced sensitivity because of both loop and chiral suppression of the induced magnetic moment operator. In the Q model, to leading order in $1/m_\chi^2$, it is given by the diagram analogous to fig. 12(b),

$$\frac{Q_b(\Lambda^\dagger\Lambda)_{bs}}{12\, m_\chi^2}\,\mathcal{O}_7 \equiv \frac{4G_F}{\sqrt{2}} V_{tb}V_{ts}^*\, C_7^{\mathrm{DM}}\,\mathcal{O}_7 \quad (30)$$

where $Q_b = -1/3$ is the charge of the b quark, and C_7^{DM} denotes the new DM contribution.

In ref. [51], a global analysis of B decay processes was performed, motivated by tensions with the SM predictions revealed by LHCb measurements [52]. There it was shown that a nonzero contribution from new physics is preferred at 1σ for $\mathcal{O}_7$, namely $C_7^{\mathrm{DM}} \in [-0.05, -0.01]$. For $m_\chi = 1$ TeV, $0.5 < (\Lambda^\dagger\Lambda)_{bs} < 2.4$ is the corresponding allowed range of couplings.

A similar analysis can be performed for the Wilson coefficient C'_7 which appears in the d model, where the 1σ range is $C_7^{\prime\,\mathrm{DM}} \in [-0.04, 0.02]$ This corresponds to the range of couplings $-0.9 < (\Lambda^\dagger\Lambda)_{bs} < 1.9$. From both C_7^{DM} and $C_7^{\prime\,\mathrm{DM}}$ the constraints on $(\Lambda^\dagger\Lambda)_{bs}$ are much weaker than the limit $|(\Lambda^\dagger\Lambda)_{bs}| < 0.19$ we obtained above from B_s-$\bar{B}_s$ mixing. Hence if one imposes the B_s-$\bar{B}_s$ mixing constraint, our DM model cannot generate large enough contributions to $B \to X_s\gamma$ decays to address the current (weak) hints of deviations from the SM predictions.

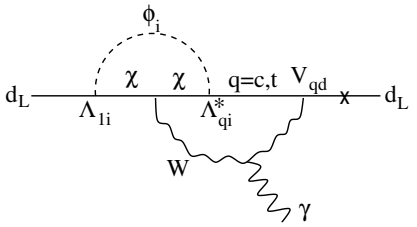

Figure 13: Diagram giving down-quark electric dipole moment.

7.3.2. $b \to s\ell^+\ell^-$

The new DM interactions contribute to $b \to s\ell^+\ell^-$ through $b \to s\gamma^*(\to \ell^+\ell^-)$ or $b \to sZ^*(\to \ell^+\ell^-)$ (i.e., the γ or Z is off-shell). All three of the operators in (29) (or their chirally-flipped counterparts) can be relevant.

There has been a great deal of activity, both theoretical and experimental, concerning $B \to K^{(*)}\mu^+\mu^-$ decays; see ref. [53] for a recent review. At present, there is a hint of new physics in C_9: at 1σ, it is found that $C_9^{\mathrm{NP}} \in [-1.6, -0.9]$, and remains nonzero even at 3σ [51]. Within the Q (d) model, we find that the $b \to s\gamma^*$ contribution to C_9 (C'_9) is

$$C_9^{\mathrm{DM}}\ (C_9^{\prime\,\mathrm{DM}}) = \frac{7\sqrt{2}Q_b(\Lambda^\dagger\Lambda)_{bs}}{144\, G_F\, m_\chi^2\, |V_{tb}||V_{ts}|}\ . \quad (31)$$

at leading order in $1/m_\chi^2$. For $m_\chi = 1$ TeV, the range of couplings $(\Lambda^\dagger\Lambda)_{bs} \in [18, 33]$ corresponds to the 1σ range of C_9^{NP}. Similarly to the case of $b \to s\gamma$, this is two orders of magnitude larger than the constraint from B_s-$\bar{B}_s$ mixing; hence the DM contribution cannot explain the discrepancy in C_9. For $C_9^{\prime\,\mathrm{DM}}$ the 1σ allowed range is $[-0.2, 0.8]$, again corresponding to constraints on $(\Lambda^\dagger\Lambda)_{bs}$ that are much weaker than those from B_s-$\bar{B}_s$ mixing.

Similar conclusions hold for all $b \to s\ell^+\ell^-$ and $b \to sq\bar{q}$ operators. The DM contribution to the Wilson coefficients is suppressed relative to the SM by $O(M_W^2/m_\chi^2) \sim 1\%$. It cannot be compensated by large values of $(\Lambda^\dagger\Lambda)_{bs}$, due to the constraint from B_s-$\bar{B}_s$ mixing.

7.4. CP violation

The couplings Λ_{ij} in our model can be complex, leading to new sources of CP violation. They can have observable effects through meson mixing in B^0 decays, and possibly also through the electric dipole moment of the neutron.

7.4.1. *Indirect CP violation in B^0 decays*

In sec. 7.1 we showed that the DM-induced contribution to B_s-$\bar{B}_s$ mixing may be significant for reasonable values of the couplings $(\Lambda^\dagger\Lambda)_{bs}^2 \sim 0.1$ in eq. (22). The

imaginary part of $(\Lambda^\dagger\Lambda)^2_{bs}$ is a new source of CP violation, entering in q/p, eq. (20),

$$\frac{q}{p} \cong \pm \left(\frac{(M_{12})^*_{\rm SM} + (M_{12})^*_{\rm DM}}{(M_{12})_{\rm SM} + (M_{12})_{\rm DM}} \right)^{1/2} . \qquad (32)$$

which is approximately a pure phase, $|q/p| \cong 1$. In the SM, $q/p = V^*_{tb}V_{ts}/V_{tb}V^*_{ts}$.

The phase $\arg(q/p)$ can be measured using indirect CP violation in B_s decays. The main experimental focus has been on $\phi_s^{c\bar{c}s}$, which is the phase as measured via indirect CP asymmetries in B_s decays with $b \to c\bar{c}s$ ($B_s \to J/\psi\phi$, $J/\psi K^+K^-$, $J/\psi\pi^+\pi^-$, $D_s^+D_s^-$). Its predicted value is $\phi_s^{c\bar{c}s} = \arg(q/p) = -0.0363^{+0.0012}_{-0.0014}$ in the SM, while the measured value is $-(0.015 \pm 0.035)$ [54]. Although these are consistent with one another, there is ample room for a new-physics contribution. Given that $(M_{12})^*_{\rm DM}$ can be of the same order as $(M_{12})^*_{\rm SM}$, our model could contribute significantly to $\phi_s^{c\bar{c}s}$.

7.4.2. CP-violation in K^0-$\bar{K}^0$, D^0-$\bar{D}^0$, B^0_d-$\bar{B}^0_d$ mixing

In contrast to the B^0_s system, the CP phase relevant for K^0-$\bar{K}^0$ and D^0-$\bar{D}^0$ mixing is sufficiently well-measured to provide a separate constraint on the imaginary part of $(\Lambda^\dagger\Lambda)_{ij}$ for the off-diagonal elements. The upper limits are given in table I. For B^0_d-$\bar{B}^0_d$ mixing, we do not present a constraint on the imaginary part of $(\Lambda^\dagger\Lambda)_{ij}$. However, its modulus is reasonably well-constrained, so that its imaginary piece cannot be too large. We therefore do not expect significant DM-induced contributions to CP violation in K^0-$\bar{K}^0$, D^0-$\bar{D}^0$, or B^0_d-$\bar{B}^0_d$ mixing.

7.4.3. Electric dipole moments

The new phases can also produce quark electric dipole moments through two-loop graphs like that shown in fig. 13. The extra loop with W exchange is needed to get the products $(\Lambda\Lambda^\dagger)_{1j}$ with $j \neq 1$, since there are no phases in $(\Lambda\Lambda^\dagger)_{11}$. Because of chiral suppression, the resulting quark EDM is small,

$$\begin{aligned} d_d \;&\sim\; \frac{{\rm Im}[(\Lambda\Lambda^\dagger)_{12}]\, e\, g_2^2\, V_{cd}\, m_d}{(16\pi^2\, m_\chi)^2} \\ &\cong\; 3\times 10^{-28}\, {\rm Im}[(\Lambda\Lambda^\dagger)_{12}]\, e\cdot{\rm cm}. \end{aligned} \qquad (33)$$

Given the stringent constraints on $(\Lambda\Lambda^\dagger)_{uc}$ and $(\Lambda\Lambda^\dagger)_{ds}$ from D^0-$\bar{D}^0$ and K^0-$\bar{K}^0$ mixing, this is negligible compared to the current sensitivity through the neutron EDM, $3\times 10^{-26}\, e$·cm.

8. BENCHMARK MODELS

Rather than trying to combine the constraints we have discussed to obtain allowed regions in parameter space, since we have many parameters, here we will instead give a few examples of allowed parameter values that illustrate the different qualitative possibilities of the model. For simplicity, we fix the mediator mass $m_\chi = 1\,$TeV, close to the lower limit from LHC searches. The benchmark models are summarized in table II.

	m_ϕ (GeV)	λ_{11}	Λ_{ij}	comment
1	60	0.01	–	asymmetric dark matter
2	63	0.016	–	GC excess
3	100	−0.12	$\Lambda_{11} = 0.04$	direct detection interference
4	200	0.08	–	thermal relic/Higgs portal
5	700	0.27	$\lvert\Lambda_{13}\rvert = 0.8$	thermal relic/mediator

Table II: Parameter values for benchmark models, assuming $m_\chi = 1\,$TeV. Dashes indicate where Λ_{ij} can take a range of values.

Model 1 underscores the fact that if the annihilation cross section exceeds that needed for the thermal relic density, then we could appeal to the complex nature of SFDM to assume that it has an asymmetry accounting for its abundance. The example chosen here has λ_{11} close to the upper limit from direct detection searches, making such a model close to discovery.

Model 2 is the largest m_ϕ below 200 GeV allowed by direct detection and the thermal relic value of λ_{11} shown in fig. 11. It is marginally consistent with the galactic center gamma ray excess, fig. 8, though in conflict with the Fermi dwarf spheroidal constraints.

Model 3 illustrates a case that would be ruled out for thermal DM but is allowed for asymmetric DM due to destructive interference between Higgs and mediator exchange contributions to DM-nucleon scattering.

Model 4 is an example where the thermal relic density arises from Higgs portal interactions, and λ_{11} is close to the LUX limit in fig. 11, again making this model detectable by the next improvement in sensitivity.

Model 5 is chosen to illustrate the window of couplings shown in fig. 7 where annihilation of dark matter by mediator exchange can dominate over the Higgs portal coupling, without fine tuning of parameters. At this mass, the LUX limit upper $\lambda_{11} < 0.5$ is satisfied. Moreover $|\Lambda_{13}|$ is below the direct detection limit ~ 2 shown in fig. 10(b). This model could be discovered with a factor of 3 improvement in direct detection sensitivity, via Higgs exchange interaction.

The sensitivity of tests from flavor-changing particle physics processes generally depends upon different parameters than the astrophysical ones considered above. For example, an observable contribution to the B^0_s-$\bar{B}^0_s$ mixing amplitude would arise from a choice of couplings such that $|\Lambda_{2s}\Lambda_{2b}| \sim 1$ in the d model. These couplings are unconstrained by the previous considerations. On the other hand it is also possible to saturate the B^0_s-$\bar{B}^0_s$ mixing bounds using $|\Lambda_{1d}\Lambda_{1b}| \sim 1$ in the same model, but the constraints from direction detection shown in fig. 10 rule out this possibility. This illustrates that there can

be some interplay between the particle physics and astrophysical constraints, but that in general there is freedom to separate them.

The nonvanishing values of Λ_{ij} required in models 3 and 5 do not have direct implications for meson mixing; rather they imply, through table I, constraints on neighboring matrix elements. For example $|\Lambda_{13}| = 0.8$ in the Q model implies $|\Lambda_{11}| < 0.02$ to satisfy B_d^0-$\bar{B}_d^0$ mixing constraints. Even if $\Lambda_{11} = 0$ at tree level, a one-loop vertex correction of order

$$\delta\Lambda_{11} \sim \frac{g^2\,\Lambda_{13}\,V_{td}}{32\pi^2} \sim 10^{-4} \tag{34}$$

is induced by $W^\pm$ exchange. Therefore no fine-tuning is needed to satisfy this constraint. Similarly $|\Lambda_{12}| = 0.04$ in the Q model requires $|\Lambda_{11}| < 0.05$ to satisfy K^0-$\bar{K}^0$ mixing constraints; this is also easily compatible with the maximum size of loop corrections.

9. CONCLUSIONS

Scalar flavored DM is somewhat more strongly constrained than its fermionic analog because of the large cross section for producing the colored fermionic mediators of SFDM at the LHC: they must typically be at the TeV scale or higher, with the possibility for lower masses $m_\chi \gtrsim 500$ GeV only if the dark matter is heavy, $m_\phi \sim 300$ GeV. As a result, many flavor-changing processes are suppressed even without any hierarchical or MFV structure in the new flavor-violating Yukawa couplings. Moreover annihilation processes relying upon mediator exchange can only be dominant for heavy DM, $m_\phi > 300$ GeV.

Also distinct from fermion FDM, scalar FDM can have important interactions through the Higgs portal. These tend to dominate in DM annihilation processes, and will be generated at one loop by the mediator couplings Λ_{ij} even if absent at tree level. We showed as a result that it is unnatural to expect mediator-dominated annihilations outside of the heavy DM mass range mentioned above. Another novel consequence is that there can be destructive interference between Higgs and mediator exchange for DM scattering on nucleons, allowing for relaxation of direct detection constraints relative to models with only one kind of interaction. This makes it possible for SFDM to be relevant for indirect detection by gamma rays from the galactic center or dwarf spheroidals, unlike for minimal scalar DM coupled through the Higgs.

Low-energy data from $\Delta F = 2$ meson mixing provide some of the most stringent constraints on the dark matter couplings, summarized in table I. The couplings Λ_{ij} for $i, j = 1, 2$ must either be very small, or very close to being diagonal. This is in contrast to the large values Λ_{i3} required if DM annihilation into top quarks is significant for determining the relic density.

There is one intriguing exception: B_s-$\bar{B}_s$ mixing. The measured values of the magnitude and phase of the mixing amplitude M_{12} are consistent with the SM predictions. However, because of large experimental errors or theoretical uncertainties, there is ample room for a new-physics contribution to M_{12}. We find that, for reasonable values of its couplings, scalar flavored DM can contribute significantly to both ΔM_s ($= 2|M_{12}|$) and the CP-violating phase β_s ($= \pm\arg(M_{12})$).

Another interesting possibility in the case of light dark matter is the apparently flavor-violating top quark decay $t \to c\,\phi_t\,\phi_c^*$, which does not rely upon any off-diagonal couplings since flavor conservation is invisibly accomplished by the dark matter flavors.

An important caveat to our analysis which could deserve further study is the simultaneous presence of mediators that couple to both left- and right-handed quarks, and which mix with each other. By excluding this more elaborate class of models, we found that all amplitudes involving mediator exchange were suppressed by $1/m_\chi^2$ (typically times a quark mass) rather than $1/m_\chi$. But in more complicated models with mediators coupling to both chiralities, one could expect much larger amplitudes involving mediators, both for DM annihilation and for FCNC processes.

Appendix A: Simulation of $\chi \to \phi t$ events

Here we give details of our simulation of the production and decay of u-like mediators that decay to DM plus top quarks. We generate events in MadGraph, interfaced with Pythia-6.4 [55] for showering and hadronization. Events are generated with up to one additional jet at the matrix-element level and matched using a shower-k_T scheme. Events are then passed to PGS [56] to simulate detector response and event reconstruction. The anti-k_T algorithm is used for jet reconstruction, with jet size parameter $R = 0.4$. Event selection is performed with cuts corresponding to the signal regions defined in ref. [20]. The same K-factor of 1.5 is applied to the cross section. We choose discrete values of the couplings so as to vary the branching fraction for decays to tops. As the branching fraction depends non-trivially on the mediator mass in the very low-mass region, we give the branching fraction as a function of the mediator mass in fig. 14, for the chosen values of the couplings. We allow for coupling to all three generations, but the distinction between first- and second-generation quarks does not affect the result, for a fixed value of the top branching fraction.

Acknowledgments: DL would like to thank J. Gaboriaud and A. Lenz for input regarding the SM contribution to B_s-$\bar{B}_s$ mixing. AD thanks Hiren Patel and Shanmuka Shivashankara for help with certain calculations. JC thanks Mike Trott for helpful discussions, and the Niels Bohr International Academy for its kind hospitality during the completion of this work. This work was financially supported by the IPP (BB), by NSERC of Canada (BB, DL, JMC, GD), by FQRNT of Québec

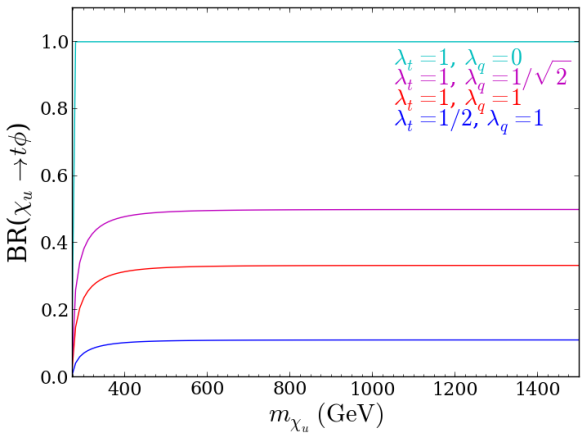

Figure 14: Branching fraction of mediator decays to top quarks, $\chi_u \to t\phi$, for chosen values of quark couplings. λ_q denotes couplings to light quarks, $\lambda_q = \lambda_u = \lambda_c$.

(JMC, GD) and by the National Science Foundation (AD) under Grant No. NSF PHY-1414345.

[1] J. Kile and A. Soni, "Flavored Dark Matter in Direct Detection Experiments and at LHC," Phys. Rev. D **84**, 035016 (2011) [arXiv:1104.5239 [hep-ph]].

[2] B. Batell, J. Pradler and M. Spannowsky, "Dark Matter from Minimal Flavor Violation," JHEP **1108**, 038 (2011) [arXiv:1105.1781 [hep-ph]].

[3] J. F. Kamenik and J. Zupan, "Discovering Dark Matter Through Flavor Violation at the LHC," Phys. Rev. D **84**, 111502 (2011) [arXiv:1107.0623 [hep-ph]].

[4] P. Agrawal, S. Blanchet, Z. Chacko and C. Kilic, "Flavored Dark Matter, and Its Implications for Direct Detection and Colliders," Phys. Rev. D **86**, 055002 (2012) [arXiv:1109.3516 [hep-ph]].

[5] A. Kumar and S. Tulin, "Top-flavored dark matter and the forward-backward asymmetry," Phys. Rev. D **87**, no. 9, 095006 (2013) [arXiv:1303.0332 [hep-ph]].

[6] L. Lopez-Honorez and L. Merlo, "Dark matter within the minimal flavour violation ansatz," Phys. Lett. B **722**, 135 (2013) [arXiv:1303.1087 [hep-ph]].

[7] B. Batell, T. Lin and L. T. Wang, "Flavored Dark Matter and R-Parity Violation," JHEP **1401**, 075 (2014) [arXiv:1309.4462 [hep-ph]].

[8] P. Agrawal, B. Batell, D. Hooper and T. Lin, "Flavored Dark Matter and the Galactic Center Gamma-Ray Excess," Phys. Rev. D **90**, no. 6, 063512 (2014) [arXiv:1404.1373 [hep-ph]].

[9] C. Kilic, M. D. Klimek and J. H. Yu, "Signatures of Top Flavored Dark Matter," Phys. Rev. D **91**, no. 5, 054036 (2015) [arXiv:1501.02202 [hep-ph]].

[10] F. Bishara, A. Greljo, J. F. Kamenik, E. Stamou and J. Zupan, "Dark Matter and Gauged Flavor Symmetries," arXiv:1505.03862 [hep-ph].

[11] D. Hooper and L. Goodenough, "Dark Matter Annihilation in The Galactic Center As Seen by the Fermi Gamma Ray Space Telescope," Phys. Lett. B **697**, 412 (2011) [arXiv:1010.2752 [hep-ph]].

[12] D. Hooper and T. Linden, "On The Origin Of The Gamma Rays From The Galactic Center," Phys. Rev. D **84**, 123005 (2011) [arXiv:1110.0006 [astro-ph.HE]].

[13] K. N. Abazajian and M. Kaplinghat, "Detection of a Gamma-Ray Source in the Galactic Center Consistent with Extended Emission from Dark Matter Annihilation and Concentrated Astrophysical Emission," Phys. Rev. D **86**, 083511 (2012) [arXiv:1207.6047 [astro-ph.HE]].

[14] B. Zhou, Y. F. Liang, X. Huang, X. Li, Y. Z. Fan, L. Feng and J. Chang, "GeV excess in the Milky Way: Depending on Diffuse Galactic gamma ray Emission template?," arXiv:1406.6948 [astro-ph.HE].

[15] T. Daylan, D. P. Finkbeiner, D. Hooper, T. Linden, S. K. N. Portillo, N. L. Rodd and T. R. Slatyer, "The Characterization of the Gamma-Ray Signal from the Central Milky Way: A Compelling Case for Annihilating Dark Matter," arXiv:1402.6703 [astro-ph.HE].

[16] F. Calore, I. Cholis and C. Weniger, "Background model systematics for the Fermi GeV excess," arXiv:1409.0042 [astro-ph.CO].

[17] S. Murgia, presented at Fifth Fermi Symposium, 20-24 Oct. 2014, http://fermi.gsfc.nasa.gov/science/mtgs/symposia/2014/program/08_Murgia.pdf

[18] G. D'Ambrosio, G. F. Giudice, G. Isidori and A. Strumia, "Minimal flavor violation: An Effective field theory approach," Nucl. Phys. B **645**, 155 (2002) [hep-ph/0207036].

[19] P. Agrawal, M. Blanke and K. Gemmler, "Flavored dark matter beyond Minimal Flavor Violation," JHEP **1410**, 72 (2014) [arXiv:1405.6709 [hep-ph]].

[20] G. Aad *et al.* [ATLAS Collaboration], "Search for squarks and gluinos with the ATLAS detector in final states with jets and missing transverse momentum using $\sqrt{s} = 8$ TeV proton–proton collision data," JHEP **1409**, 176 (2014) [arXiv:1405.7875 [hep-ex]].

[21] J. Alwall *et al.*, "The automated computation of tree-level and next-to-leading order differential cross sections, and their matching to parton shower simulations," JHEP **1407**, 079 (2014) [arXiv:1405.0301 [hep-ph]].

[22] A. Alloul, N. D. Christensen, C. Degrande, C. Duhr and

B. Fuks, "FeynRules 2.0 - A complete toolbox for tree-level phenomenology," Comput. Phys. Commun. **185**, 2250 (2014) [arXiv:1310.1921 [hep-ph]].

[23] G. Aad *et al.* [ATLAS Collaboration], "Measurement of the top pair production cross section in 8 TeV proton-proton collisions using kinematic information in the lepton+jets final state with ATLAS," Phys. Rev. D **91**, no. 11, 112013 (2015) [arXiv:1504.04251 [hep-ex]].

[24] M. Cacciari, M. Czakon, M. Mangano, A. Mitov and P. Nason, "Top-pair production at hadron colliders with next-to-next-to-leading logarithmic soft-gluon resummation," Phys. Lett. B **710**, 612 (2012) [arXiv:1111.5869 [hep-ph]].

[25] G. Steigman, B. Dasgupta and J. F. Beacom, "Precise Relic WIMP Abundance and its Impact on Searches for Dark Matter Annihilation," Phys. Rev. D **86**, 023506 (2012) [arXiv:1204.3622 [hep-ph]].

[26] J. M. Cline, K. Kainulainen, P. Scott and C. Weniger, "Update on scalar singlet dark matter," Phys. Rev. D **88**, 055025 (2013) [arXiv:1306.4710 [hep-ph]].

[27] M. Ackermann *et al.* [Fermi-LAT Collaboration], "Searching for Dark Matter Annihilation from Milky Way Dwarf Spheroidal Galaxies with Six Years of Fermi-LAT Data," arXiv:1503.02641 [astro-ph.HE].

[28] T. A. Porter *et al.* [for the Fermi LAT Collaboration], "Observations of High-Energy Gamma-Ray Emission Toward the Galactic Centre with the Fermi Large Area Telescope," arXiv:1507.04688 [astro-ph.HE].

[29] I. Cholis, C. Evoli, F. Calore, T. Linden, C. Weniger and D. Hooper, "The Galactic Center GeV Excess from a Series of Leptonic Cosmic-Ray Outbursts," arXiv:1506.05119 [astro-ph.HE].

[30] R. Bartels, S. Krishnamurthy and C. Weniger, "Strong support for the millisecond pulsar origin of the Galactic center GeV excess," arXiv:1506.05104 [astro-ph.HE].

[31] T. D. Brandt and B. Kocsis, "Disrupted Globular Clusters Can Explain the Galactic Center Gamma Ray Excess," arXiv:1507.05616 [astro-ph.HE].

[32] J. M. Cline, G. Dupuis, Z. Liu and W. Xue, "Multimediator models for the galactic center gamma ray excess," Phys. Rev. D **91**, no. 11, 115010 (2015) [arXiv:1503.08213 [hep-ph]].

[33] M. Cirelli *et al.*, "PPPC 4 DM ID: A Poor Particle Physicist Cookbook for Dark Matter Indirect Detection," JCAP **1103**, 051 (2011) [JCAP **1210**, E01 (2012)] [arXiv:1012.4515 [hep-ph], arXiv:1012.4515 [hep-ph]].

[34] D. S. Akerib *et al.* [LUX Collaboration], "First results from the LUX dark matter experiment at the Sanford Underground Research Facility," Phys. Rev. Lett. **112**, 091303 (2014) [arXiv:1310.8214 [astro-ph.CO]].

[35] A. L. Fitzpatrick, D. Hooper and K. M. Zurek, "Implications of CoGeNT and DAMA for Light WIMP Dark Matter," Phys. Rev. D **81**, 115005 (2010) [arXiv:1003.0014 [hep-ph]].

[36] A. Hamze, C. Kilic, J. Koeller, C. Trendafilova and J. H. Yu, "Lepton-Flavored Asymmetric Dark Matter and Interference in Direct Detection," Phys. Rev. D **91**, 035009 (2015) [arXiv:1410.3030 [hep-ph]].

[37] M. L. Graesser, I. M. Shoemaker and L. Vecchi, "Asymmetric WIMP dark matter," JHEP **1110**, 110 (2011) [arXiv:1103.2771 [hep-ph]].

[38] For example, see I. Dunietz and J. L. Rosner, "Time Dependent CP Violation Effects in B0 anti-B0 Systems," Phys. Rev. D **34**, 1404 (1986).

[39] A. Lenz *et al.*, "Anatomy of New Physics in $B - \bar{B}$ mixing," Phys. Rev. D **83**, 036004 (2011) [arXiv:1008.1593 [hep-ph]].

[40] G. Isidori, Y. Nir and G. Perez, "Flavor Physics Constraints for Physics Beyond the Standard Model," Ann. Rev. Nucl. Part. Sci. **60**, 355 (2010) [arXiv:1002.0900 [hep-ph]].

[41] A. Lenz, private communication.

[42] R. Goldouzian [CDF and D0 and ATLAS and CMS Collaborations], "Search for FCNC in top quark production and decays," arXiv:1412.2524 [hep-ex].

[43] T. Li and Q. Shafi, "Scalar Dark Matter Search at the LHC through FCNC Top Decay," Phys. Rev. D **83**, 095017 (2011) [arXiv:1101.3576 [hep-ph]].

[44] X. G. He, T. Li, X. Q. Li and H. C. Tsai, "Scalar dark matter effects in Higgs and top quark decays," Mod. Phys. Lett. A **22**, 2121 (2007) [hep-ph/0701156].

[45] L. B. Jia, "Search for pseudoscalar-mediated WIMPs in $t \to c$ transitions with missing energy," arXiv:1506.05293 [hep-ph].

[46] G. Aad *et al.* [ATLAS Collaboration], "Search for FCNC single top-quark production at $\sqrt{s} = 7$ TeV with the ATLAS detector," Phys. Lett. B **712**, 351 (2012) [arXiv:1203.0529 [hep-ex]].

[47] G. Aad *et al.* [ATLAS Collaboration], "Search for single top-quark production via flavour changing neutral currents at 8 TeV with the ATLAS detector," arXiv:1509.00294 [hep-ex].

[48] CMS Collaboration [CMS Collaboration], "Search for anomalous single top quark production in association with a photon," CMS-PAS-TOP-14-003.

[49] S. Chatrchyan *et al.* [CMS Collaboration], "Search for Flavor-Changing Neutral Currents in Top-Quark Decays $t \to Zq$ in pp Collisions at $\sqrt{s} = 8$TeV," Phys. Rev. Lett. **112**, no. 17, 171802 (2014) [arXiv:1312.4194 [hep-ex]].

[50] V. Khachatryan *et al.* [CMS Collaboration], "Searches for heavy Higgs bosons in two-Higgs-doublet models and for tch decay using multilepton and diphoton final states in pp collisions at 8 TeV," Phys. Rev. D **90**, 112013 (2014) [arXiv:1410.2751 [hep-ex]].

[51] S. Descotes-Genon, J. Matias and J. Virto, "Understanding the $B \to K^* \mu^+ \mu^-$ Anomaly," Phys. Rev. D **88**, 074002 (2013) [arXiv:1307.5683 [hep-ph]].

[52] R. Aaij *et al.* [LHCb Collaboration], "Measurement of Form-Factor-Independent Observables in the Decay $B^0 \to K^{*0} \mu^+ \mu^-$," Phys. Rev. Lett. **111**, 191801 (2013) [arXiv:1308.1707 [hep-ex]].

[53] S. Descotes-Genon, L. Hofer, J. Matias and J. Virto, "Theoretical status of $B \to K^* \mu^+ \mu^-$: The path towards New Physics," J. Phys. Conf. Ser. **631**, no. 1, 012027 (2015) [arXiv:1503.03328 [hep-ph]].

[54] Y. Amhis *et al.* [Heavy Flavor Averaging Group (HFAG) Collaboration], "Averages of b-hadron, c-hadron, and τ-lepton properties as of summer 2014," arXiv:1412.7515 [hep-ex].

[55] T. Sjostrand, S. Mrenna and P. Z. Skands, "PYTHIA 6.4 Physics and Manual," JHEP **0605**, 026 (2006) [hep-ph/0603175].

[56] J. Conway, Pretty Good Simulation of high energy collisions, `http://physics.ucdavis.edu/~conway/research/software/pgs/pgs4-general.htm`